We are IntechOpen, the world's leading publisher of Open Access books Built by scientists, for scientists

4,800
Open access books available

122,000
International authors and editors

135M
Downloads

Our authors are among the

154
Countries delivered to

TOP 1%
most cited scientists

12.2%
Contributors from top 500 universities

CLARIVATE ANALYTICS BOOK CITATION INDEX INDEXED

WEB OF SCIENCE™

Selection of our books indexed in the Book Citation Index in Web of Science™ Core Collection (BKCI)

Interested in publishing with us?
Contact book.department@intechopen.com

Numbers displayed above are based on latest data collected.
For more information visit www.intechopen.com

Chapter 5

Holographic Sensors for Detection of Components in Water Solutions

Vladimir A. Postnikov, Aleksandr V. Kraiskii and Valerii I. Sergienko

Additional information is available at the end of the chapter

http://dx.doi.org/10.5772/53564

1. Introduction

Currently optical sensors for measuring considerable concentrations of specific components of solutions and their parameters attract persistent worldwide interest. One of the advantages of these sensors is that they permit one to determine simply concentrations both instrumentally and visually. These sensors include holographic sensors [1, 2] and photonic crystal sensors [3, 4]. They can be used for measuring the concentration of protons (pH) in water solutions, heavy metal ions [5-8], glucose in blood [7-12] and other biological liquids [13,14], bacterium spores [15,16], metabolites [17] bacterial growth [18,19], humidity and temperature responses [20,21].

Holographic sensors are quite promising because they are highly sensitive, are easy to operate, provide high enough accuracy and can be used for various applications. At present time they belong to sensors with a moderate sensitivity (10^{-5} -10^{-1} mol•L^{-1}), depending on the type of the analyzed component, the design and the composition of the sensor matrix. Such a sensitivity range is required, for example, in measurements of the glucose concentration in blood and other biological liquids. Holographic sensors represent a polymer hydrogel matrix grafted onto the surface of glass or transparent polymer films and doped with nanosize solid grains, so that their concentration changes periodically in space and the mean distance between the grains is much smaller than the visible-light wavelength.

Holographic diffraction gratings [22] are generated within photosensitive polymer-silver halide photographic emulsions upon exposure to a single collimated laser beam, which passes through the polymer film and then reflected back by a plane mirror. Interference between the mutually coherent incident and reflected beams generates a standing wave pat-

tern which, after development and fixing, creates a three-dimensional pattern comprising fringes of ultrafine metallic silver grains embedded within the thickness (from 5 to 50 μm) of the polymer film. Under white light illumination, the holographic fringes reflect light of a specific narrow band of wavelengths, hence acting as a sensitive wavelength filter and recreating a monochromatic image of the original mirror used in their construction. Constructive interference between partial reflections from each plane produces a distinctive spectral peak with a wavelength governed by the Bragg equation ($m\lambda_{max} = 2n\ d\ sin\theta$). Any physical, chemical, or biological reaction that that alters the spacing (d) between fringes or the refractive index (n) will generate visible changes in the wavelength (color) or intensity (brightness) of the reflection hologram. The intensity of holographic diffraction is also determined by the number of planes and the modulation depth of the refractive index. Swelling of the holographic film increases the distance between fringes producing a red-shift in the wavelength of reflected light, whereas film shrinkage results in a blue-shifted light. In essence, the holographic gratings act as a reporter, whose optical properties are dictated by the physical characteristics of the holographic film. Reflection holograms have proven to be advantageous in many aspects, including the simplicity bestowed by the holographic element providing both the analyte-sensitive matrix and the optical transducer. Special components embedded into the hydrogel matrix to cause a change in the swelling (or shrinkage) of hydrogel under the action of component solution to be analyzed. This leads to the change in the period of the structure and, therefore, in the reflected radiation wavelength. By measuring this wavelength with the help of an optofibre spectrometer or observing it visually, we can estimate the concentration of tested components (metal ions, glucose, acidity, etc.).

The main goal at this stage is the development of sensors for measuring the glucose concentration in blood - low-cost and simple to handle of test plates. In addition, we assume the possibility of the development of sensors to control the conditions of transport and storage of vaccines, serums, ferment preparations, food, and also simple test systems in homes. In our opinion, the study of mechanisms of changes in the holographic response will make it possible to perform the precise adjustment of a sensor for particular operating conditions.

2. Results and discussion

Photosensitized nanocrystals of AgBr were synthesized in the hydrogel matrix by diffusion method [2]. By exposing photographic emulsions in water or acetic acid (1%) solution to radiation from a He-Ne (632.8 nm, 15 mW) laser in the counter propagating-beam scheme, we obtained silver nanograins [23-28] with the period of layers providing the location of reflected radiation peaks in the operating region of the spectrometer. A number of matrices of different compositions and designs were investigated. Hydrogel matrices were consisted of three-dimensional polymer of acrylamide (AA), N, N'-methylene-bis-acrylamide (bis) as crosslinking agent and other comonomers: N-ε-methacryloyl-lysin (Lys), 2-(dimethylamino)-ethylmethacrylate (DMA), acrylic acid (AC), N-acryloyl-2-glucosamine (GA), N-acryloyl-3-aminophenylboronic acid (AMPh). Matrices based on copolymers of acrylamide with

http://dx.doi.org/10.5772/53564

ionogen comonomers are sensitive to the solution acidity and ionic strength, while matrices based on aminophenylboronic acid are sensitive to glucose.

Figure 1 shows the typical reflection spectrum of the sensitive layer of a sensor. The reflection spectrum for the ideal layer should be described by the function $(\sin x/x)^2$. In our case, the spectrum is well described by a Gaussian. This is explained apparently the imperfect arrangement of silver grain layers.

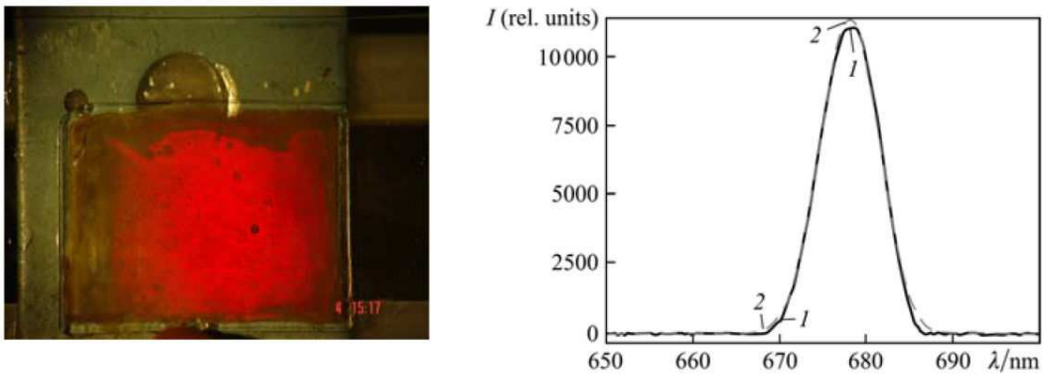

Figure 1. The experimental reflection spectrum of the sensor (1) and its approximation by a Gaussian of width 8 nm (2). (Sensor: AA-AMPh-bis – 87-12-1 mol.%,)

Note that metal silver grains are located in the hologram in a very complex environment containing molecules and ions of solution, elements of the hydrogel matrix. When the solution composition is changed, the composition of ions in solution and the structure of the matrix itself are redistributed. As a result, the sensor response, i.e. the mean wavelength of reflected radiation changes, and the radiation intensity also changes due to the change in the diffraction efficiency of the hologram.

One of the most important properties of holographic sensors is reversibility of the response when changing composition of the solution (Fig.2). Figure 2a shows the time dependence of the reflection line shape during the transfer of the sensor based on aminophenylboronic acid from the citrate buffer to distilled water and back. This change is reversible. The complex shape of the line is explained by the inhomogeneous distribution of the distance between silver layers over depth. One can see that the diffraction efficiency decreases during layer swelling. Figure 2b presents the time dependences of the reflection line wavelength for aminophenylboronic acid sensor after the replacement of the alkali solution in a cell by the acid solution and vice versa (transition processes). The wavelength was measured during swelling and transition to the stationary state. In this case, the swelling changes monotonically and approximately exponentially. Figure 3 shows the time dependence of the reflection wavelength in the transition process after the replacement of the citrate buffer by distilled water. The initial state of this sensor was not stationary. The time dependences of the reflection wavelength and intensity are nonmonotonic, their signs being opposite. The nonmonotonic behavior can be explained by the complicated character of variations ionic composition of solution in the emulsion. It

can be assumed that at the initial moment there is rapid diffusion of hydrogen ions from the hydrogel matrix. Then the dissociation of aminophenylboronic acid take place and negative charge appear on polymer chains. This leads to an increase in the period of the holographic grating and is accompanied by an increase in the wavelength of reflected light. The larger anion citrate diffuses slowly, and the system is gradually coming to an equilibrium state, which is accompanied by compression of the hydrogel matrix and decreasing the wavelength of the reflected light. The observed change in intensity, appear to reflect the change in the microenvironment of silver particles. This effect requires additional studies.

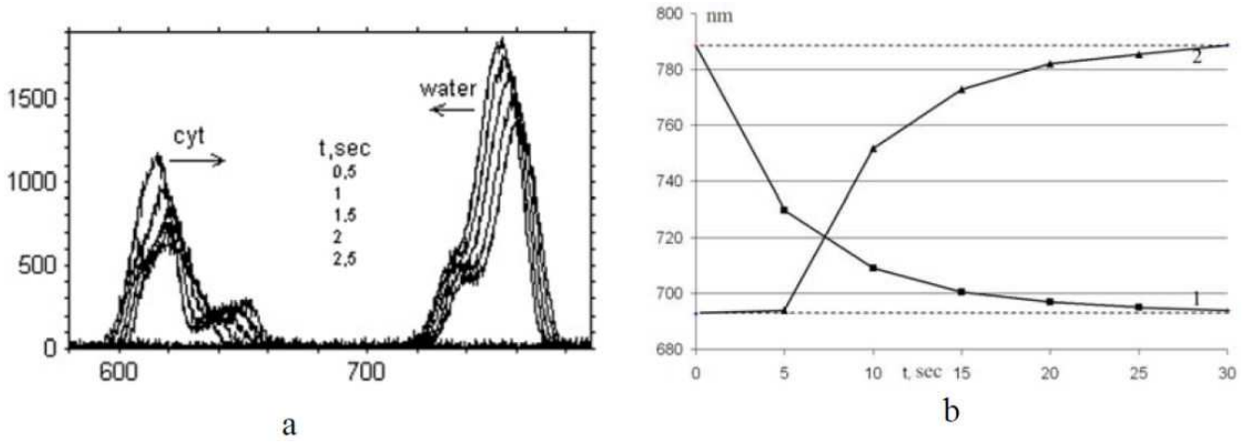

Figure 2. a) Change in the reflection line shape during the transfer of a sensor from the citrate buffer to distilled water (on the right) and back (on the left). The time step is 0.5 s. The arrows indicate the direction of the line shift in time for each group of the lines. b) Refection line wavelengths during the transfer of a sensor based on aminophenylboronic acid from alkali to acid [shrinkage, (1)] and vice versa [swelling, (2)]. (Sensor: AA-AMPh-bis – 87-12-1 mol.%,)

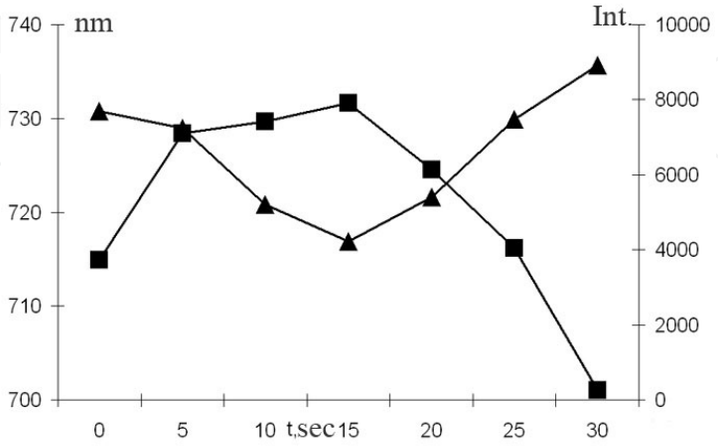

Figure 3. The reflection wavelength line (■) and intensity (▲) during the transfer of the sensor based on aminophenylboronic acid from the citrate buffer to distilled water (b).

http://dx.doi.org/10.5772/53564

Figure 4a shows the response of the sensor located in the NaOH solution titrated hydrochloric acid with (the solution acidity was measured with a usual pH-meter). During titration, the reflected radiation wavelength and diffraction efficiency change drastically at the point where the solution acidity drastically changes. In this case, the diffraction efficiency changed almost by an order of magnitude. This means that the change in the ionic composition is accompanied not only by the swelling of hydrogel matrix of the sensor but also by a strong change in the scattering properties of a holographic layer. This fact was unknown before our studies. Figure 4b presents the dependences from Fig. 4a reduced to the same scale by using the following algorithm. For some dependence $F(m)$, we determined the maximum (A) and minimum (B) of its values for the boundary values of its argument m (in Fig. 4, the volume of the added acid solution): $A = \max(F(0), F(mmax))$, $B = \min(F(0), F(mmax))$. Then, the dependence $F(m)$ was transformed to the dependence $f(m)$ as $f(m) = (F(m) - B)(A - B)$. One can see from Fig. 4b that all the features of the titration curve are reflected in optical characteristics, i.e. they can be used to control the acidity. Note that the sign of a change in the diffraction efficiency during a change in the amount of added acid is opposite to the sign in the wavelength change.

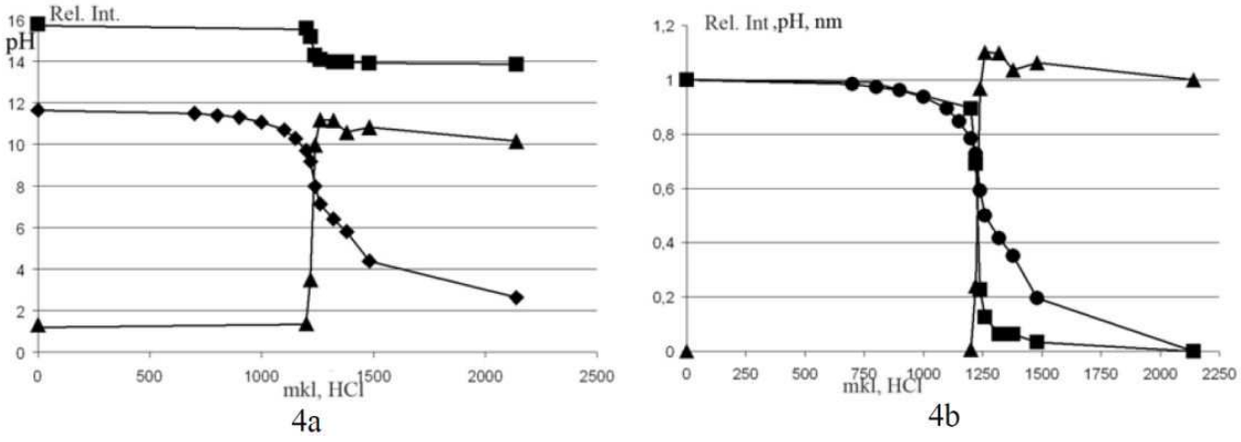

Figure 4. Dependences of the acidity (measured in solution) (◆-a,●-b), the wavelength (■), and intensity (▲) of radiation reflected from a sensor in the NaOH (0,01 N) solution during its titration with hydrochloric acid (0,1 N) (a) and also the so-called reduced dependences (see the text) (b). (Sensor: AA-AC-bis – 96-3-1 mol.%,)

Figure 5 shows the responses of sensors with acrylic acid to metal ions in a broad concentration range from 10^{-7} to 10^{-1}M. They can be divided into three groups: 1- Pb, Co^{+} ions; 2- other bivalent metal ions; 3- alkali metal ions. The sensor is most sensitive to Pb^{2+} and Co^{3+} ions (10^{-5} M). Among the bivalent metal ions (Mg, Sr, Mn, Pb), the presence of Pb^{2+} ions in the solution led to the most noticeable contraction of the hydrogel and changes (542 nm, 37% contraction). The reflection maximum was shifted down by 320 nm with respect to that of the distilled water. The sensor sensitivity to Mg^{2+}, $Sr^{2+}$and Mn^{2+} ions was two orders of magnitude lower. Note that, unlike other metal ions, the sensor's response to the alkali metal ions (Na^{+}, K^{+}) is changed - the first wavelength increases (swelling of hydrogel occurs) and then decreases (shrinkage).

The sensor with acrylic acid can be used for determining the presence of metal ions in water (Fig.6). Figure 6a presents the reflection spectra of the sensor located in different solutions. Stationary response for distilled water is λ=735 nm while response for tap water - λ=615.2 nm which we explain by the presence of metal ions in tap water. The maxima of the reflection lines in water after filtration by household filters are located at 676 nm (Barrier filter) and 711.7 nm (Aquafor filter). The response of sensor on tap water is closer to position for mineral water containing calcium salt at concentration $3 \cdot 10^{-3}$ M (λ=585.4 nm) and to lead salt ($5 \cdot 10^{-3}$ M) in distilled water (λ=542 nm). Sensors can be used repeatedly after regeneration, by washing them, for example, in sodium citrate and then in distilled water. A sensor response rapidly passes to the IR region (λ=860 nm) and then slowly passes to the stationary state (735 nm). Figure 6b shows the typical kinetics of the response maximum.

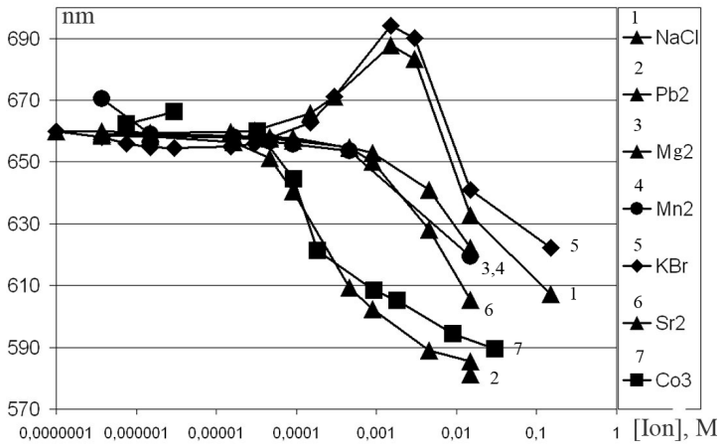

Figure 5. The sensors response (λ_{max}) on different metal ions (1-7) in water solution. (Sensor: AA-AC-bis – 96-3-1 mol.%,)

Fig.7 shows the responses of sensors for matrices of two types (with AC or AMPh) for different concentrations of ethanol in water. Figure 7a presents the reflection lines of a sensor based on acrylic acid for different concentrations of ethanol in water, while Fig. 7b shows the dependences of the reflection line wavelength on the ethanol concentration for this sensor and a sensor based on aminophenylboronic acid. The wavelength of reflected light at zero EtOH concentration depends both on the properties of the sensor matrix and on the recording conditions of holograms and can be changed in a controllable way within some range. The concentration dependence in the ethanol solution differs from that upon titration because in this case the decrease in swelling is probably caused by simple dehydration of solution inside the matrix, without ionization.

The spectral region of the sensor's response can be modified in various ways: changing the composition of the solution in the recording hologram (swelling of the hydrogel matrix to change), using a laser at a different wavelength (e.g., instead of the He-Ne laser - semiconductor lasers with an appropriate photosensitizer) or changing the composition of the hydrogel matrix. This can be performed by varying the matrix design and selecting proper co-monomers and their concentrations. Figure 8 shows the dependences of

http://dx.doi.org/10.5772/53564

the reflection line wavelength on the solution acidity for matrices of different compositions. One can see that the properties of the sensor response can be controlled in a broad range. Differences in the response of these sensors at titration of HCl solution correspond to pK_a of components in polymeric matrices, when the charge changes and matrices swelling (or shrinkage) take place. Thus, we have instruments to influence on wavelength maximal response of the holographic system with aminophenylboronic acid from 450 nm (Lys) to 720 nm (DMA) at pH 7.4 (pH of blood serum). The response of the sensor AA-AMPh-GA pointed to the fast swelling when the pH solution is approaching to pK_a= 8.9 aminophenylboronic acid and following slowly shrinkage of the polymeric matrix, at pH more 9.2 – only the swelling. The optical response can be a consequence of a number of different processes: diffusion of H^+ out the gel, complex formation between GA and AMPh groups, and structural rearrangements of the gel due to the increasing concentration of negative charges resulting in gel hydration and swelling.

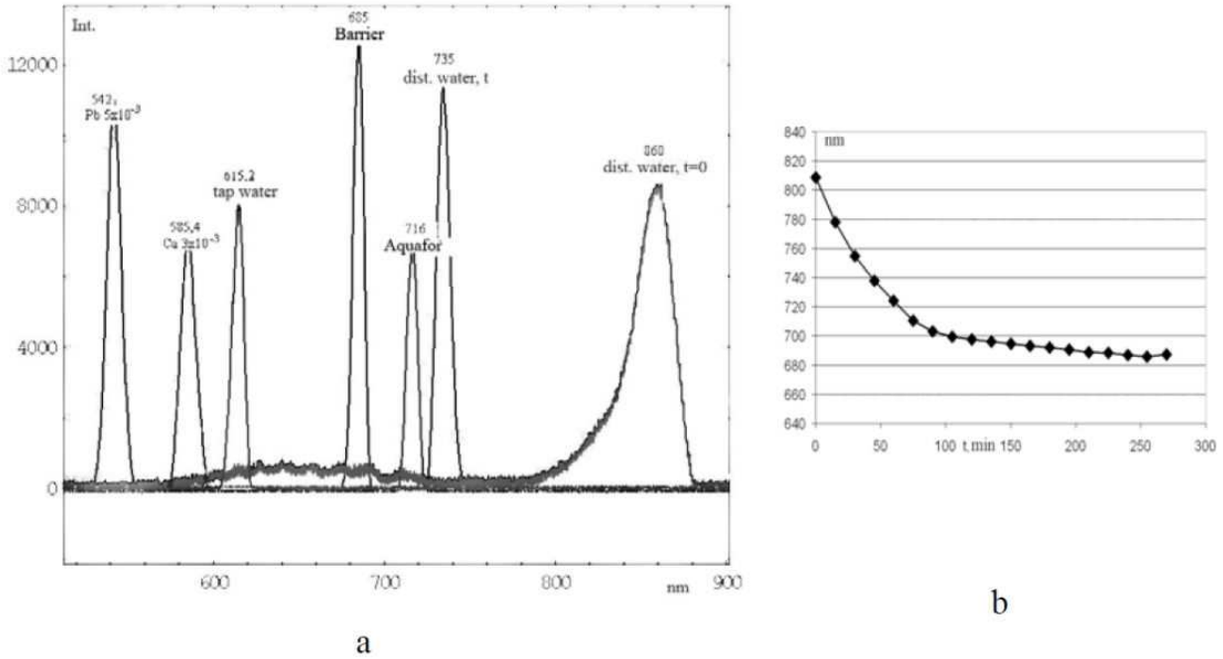

Figure 6. Sensors response to metal ions in water. Reflection spectra in distilled water after the transfer of the sensor from the citrate solution (λ = 860 nm); distilled water (stationary state) (λ = 724 nm); tap water after an Aquafor filter (λ = 711,7 nm); tap water after Barrier filter (λ = 676.3 nm); cold tap water (λ = 615,2 nm); mineral water containing $[Ca^{2+}]$ $3 \cdot 10^{-3}$ M (λ = 585.4 nm); lead salt solution in distilled water $[Pb^{2+}]$ $5 \cdot 10^{-3}$ M (λ = 542 nm) (a) and the shift of the response wavelength of a sensor in distilled water to the stationary state after regeneration (6b). (Sensor: AA-AC-bis – 96-3-1 mol.%,)

It is known that boronic acid can reversibly interact with 1,2-diols or 1,3-diols in aqueous solution to form 5- or 6-membered ring cyclic esters [27-30], (Fig.9). The neutral trigonal form of boronic acid molecules transforms into the anionic tetrahedral form on binding a saccharide, upon which a proton is released. Ester formation by interaction of the corresponding arylboronate with a diol is known to occur very fast and reversibly in aqueous media. Five and six membered cyclic arylboronate esters are formed upon binding between

arylboronic acids and cis-1,2- or 1,3-diols respectively. With d-glucose the boronic acid has a choice of binding either the 1,2- or 4,6-diols, but with d-glucosamine hydrochloride, binding with just the 4,6-diol is possible. The stability constant with d-glucose is higher than that observed with d -glucosamine hydrochloride. It may be assumed that this behavior agrees with binding GA with tetrahedron B^--atoms of boronic acid that carry into effect of additional crosslinking.

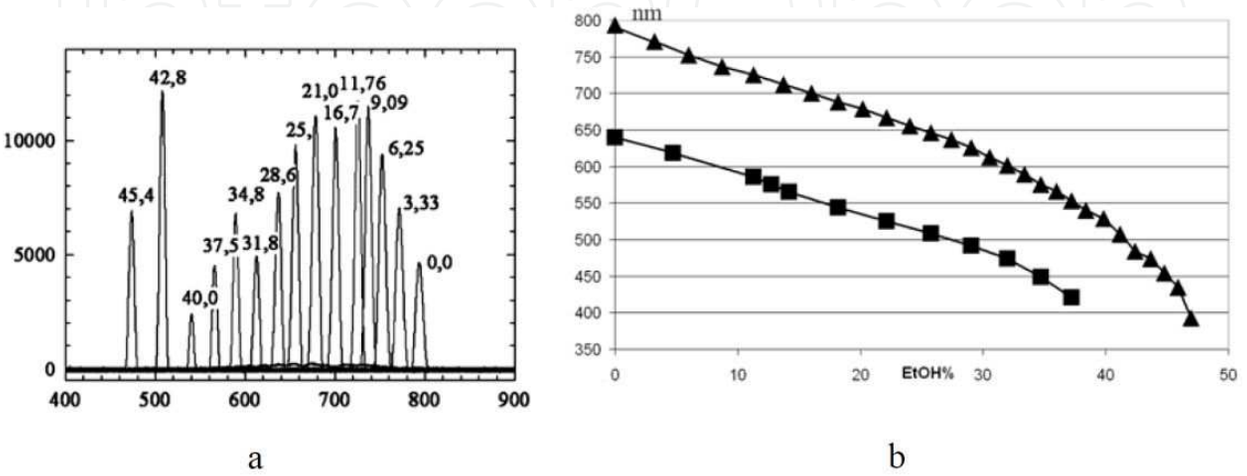

Figure 7. Reflection spectra of sensor based on acrylic acid (AA-AC-bis – 97.8-1.3-0.9 mol.%) at different concentrations of ethanol solutions (a) and the reflection line wavelengths for sensor based on acrylic acid (AA-AC-bis - 97.8-1.3-0.88 mol.%) (upper curve) and aminophenylboronic acid (AA-AMPh-bis – 98-1-1 mol%) (lower curve) (b).

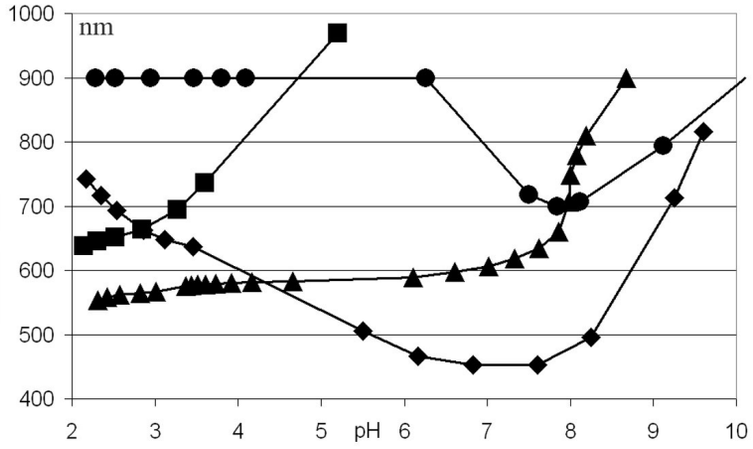

Figure 8. Dependences of the reflection line wavelength on the solution acidity for matrices of different compositions. (sensors: AA-AMPh(12 mol.%)-X-bis; X: ■-AC (5.8, bis-3 mol.%) ●-DMA (3.6, bis -3 mol.%, ▲-GA(3.6, bis-1, mol. %), ◆-Lys (5.8, bis-1 mol.%))

The quantitation of glucose is among the most important analytical tasks. It has been estimated that about 40% of all blood tests are related to it. In addition, there are numerous other situations where glucose needs to be determined, for example in biotechnology, in the

http://dx.doi.org/10.5772/53564

production and processing of various kinds of feed and food, in biochemistry in general, and other areas. The significance of glycemic control for the prevention of diabetes complications is well established [30]. The market for glucose sensors probably is the biggest single one in the diagnostic field, being about 30 billion $ per year today. Given this size, it is not surprising that any real improvement in glucose sensing (in whole blood and elsewhere) represents a major step forward. Holographic glucose sensors represent a comparatively new development [9-12, 18, 26]. The advantage of the holographic method over other optical techniques is the long-term stability of the sensor and the ease with which the wavelength may be tuned to suit the application.

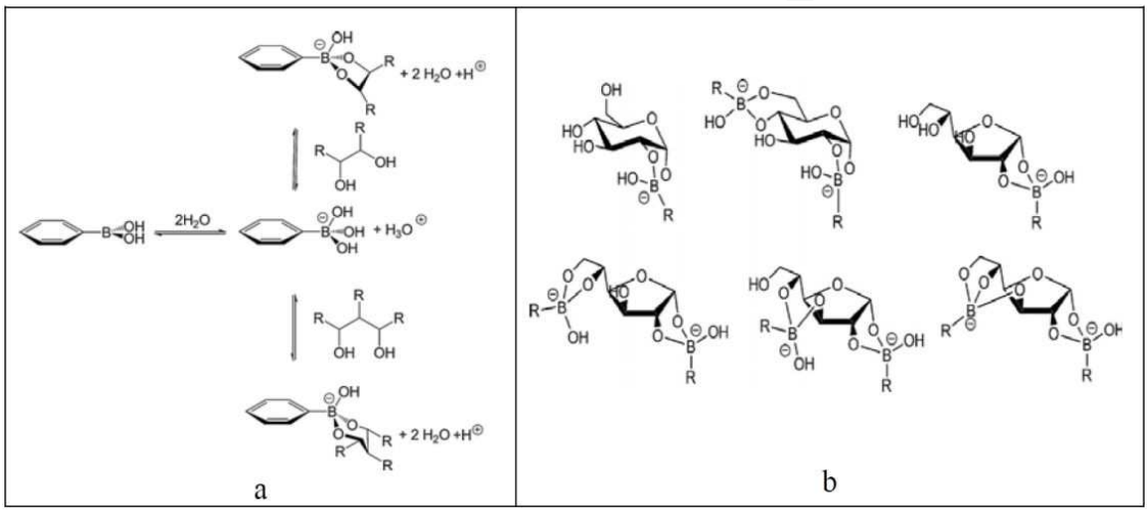

Figure 9. The spontaneous ester formation between phenylboronate and cis-1,2-diol or 1,3-diol compounds (a), arylboronate complexes formed with d-glucose (b) [29]

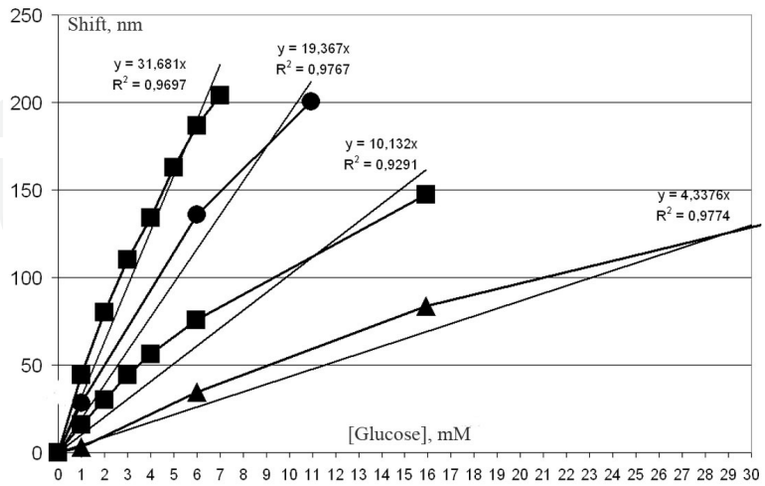

Figure 10. Dependences of the reflection line wavelength on the glucose concentration for different sensors. The straight lines are approximations of experimental curves by proportional functions described by presented equations with determination coefficients R^2. (sensors: AA with AMPh- GA-bis, mol.%:▲- 4-1-0.5, ■- 4-1-0.1, ● -12-0-1, ◙ -6-6-0.1mol.%; 0,01 M glycine, pH 7.4)

Sensors with aminophenylboronic acid were sensitive to glucose concentrations in the solution. The reflection (λ_{max}) and the shift (λ_0-λ_{max}) were influenced on the additive to polymer net, the buffer solution and pH. The shift of λ_{max} is changed from 10 to 200 nm when glucose concentration was increased (0-30 mM). By investigating the properties of sensors in detail, we optimized responses of sensors to glucose. Their concentration dependences are shown in Fig.10.

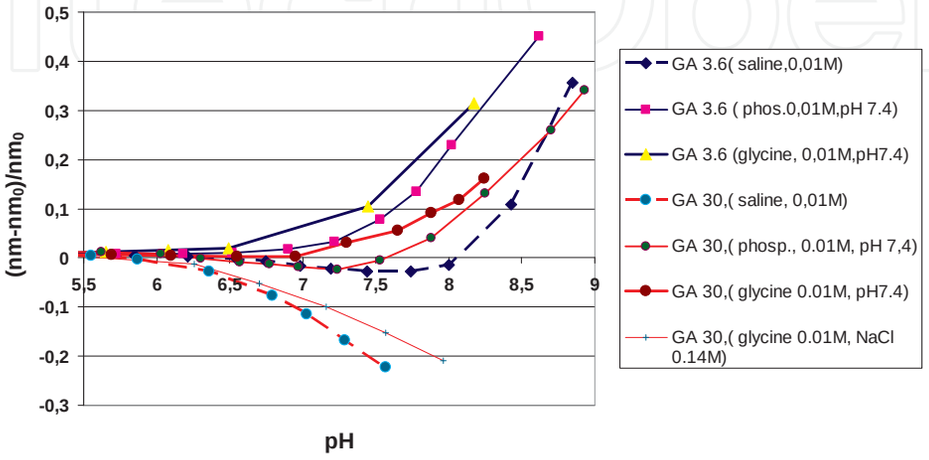

Figure 11. The influence of ionic strength on the hydrogels shrinkage in solutions. (Sensors: AA with GA-AMPh-bis-3.6-12-1; 30-12-1, mol.%)

One can see that the sensor sensitivity changes from 4.3 to 32 nm/(mmol·L^{-1}). Copolymer of acrylamide containing 6 mol.% glucosamine, 6 mol.% boronic acid, 0.1 mol.% bis shows the most sensitivity in glycine solution, pH 7.4. The response of sensor to glucose in blood serum is lower but allows to distinguish changes in 1 mM glucose concentration. A possible reason for reducing the sensitivity of sensors to glucose in the blood serum is a contraction of the matrix caused by ionic strength. According to Fig. 11 at pH = 7.4 for all sensors including the GA and AMPh with increasing content of sodium ions to 0.14 M in the solution, there is a significant contraction of the hydrogel (20%). Therefore swelling of the hydrogel due to the presence of glucose occurs in the already highly compressed hydrogel

Holographic sensors give an interesting object in study of light scattering by an ensemble of nanoparticles, since one can change the environment of the particles almost preserving their mutual location. In these systems (see Fig. 4) we found that when the concentration of alkali changes in the titration, at the same time a sharp change in pH occurs, as well as a sharp change in the position of maximum reflection and a sharp and significant (almost by an order of magnitude) change in the diffraction efficiency of the holographic sensor. This indicates a significant change of the optical characteristics of the holographic layer [28, 33]. These characteristics include diffraction effectivity (DE), transmission, spectral form of the reflection line (in particular, its width) and wavelength distribution over the hologram surface. The line shape reflects homogeneity of the layer period into depth of the hologram. Its study allows investigating the transition processes in emulsion under change of solution.

http://dx.doi.org/10.5772/53564

The transmittance and the line width together allow one to determine the effective number of layers and the weak inhomogeneity of the period. The processes in the sensitive hologram layer when changing solution parameters are complicated due to changing the molecular and ion structure in the solution within the hydrogel, to re-constructing the gel matrix, to interaction of the light-scattering grains with the solution components and matrix elements. Hologram based on silver nanoparticle layers is a typical nanoplasmonics object which scatters light in a complicated environment of ions of different kinds, of water molecules and of polymer matrix elements. The emulsion matrix interacts with the tested compounds by changing the density of crosslink in the polymer mesh. This may change as the charge distribution in the matrix and the composition of ions and other components in the solution. All of these elements (matrix elements, ions, molecules of the solution), interacting with each other and with silver nanograins, can alter the dynamic characteristics of electronic subsystems that match the light field, which leads to a change in optical characteristics. The research of these characteristics would help to understand the processes inside the emulsion and in the vicinity of nanograins.

If the period of layers is constant in depth and the modulation is weak (transmittance of a layer at the resonant wavelength λ is close to unity), the spectral width $\Delta\lambda$ of the reflection line is inverse proportional to the thickness H of the sensitive layer, or to the number of periods N:

$$\Delta\lambda = 0.866\lambda^2 / 2n_0 H = 0.866\lambda / N$$

where n_0 is the mean index refraction of holographic layer. The accuracy of determination of wavelength depends on this value. This formula is valid only when the conditions described above. In all other cases require special methods of calculation [33].

The mode of sensor operation is very important. A good resolution is obtained when all the sensitive layer work effectively. If the falling radiation cannot penetrate sufficiently deep, the effective thickness of the hologram decreases. It reduces the resolution. Typically, the sensor sensitive layer contains silver nanograins, which have a high refractive index and a high absorption coefficient in the visible region of the spectrum. This leads to the elimination of radiation from the plane wave of light illuminating the hologram, due to absorption and scattering. This also reduces the number of effectively operating layers and, consequently, leads to the broadening of the reflection spectral line and to the deterioration of accuracy. The increase of the amplitude of modulation of the refractive index, which is introduced to increase the diffraction efficiency of the hologram, leads to the same effect. On the other hand, a strong decrease of the modulation amplitude narrows the line to the limit, but decreases the diffraction efficiency and, consequently, the measurement accuracy. Obviously, the parameters can be optimized. Therefore one needs a rather accurate method of determining the parameters of the hologram.

One of the important reasons to study optical properties of holographic sensors is to provide the proper work regime of the sensor. That means that the holographic sensor should work in the whole working range of concentrations as a thin photonic crystal (the reflectance is weak).

The hologram functioning depends seriously upon the light scattering properties. In its turn, these depend on both the type (metal or dielectric) and properties of the scattering center, and on its environment (mixture and ion concentration of the solution and of the hydrogel). The light scattering is the Raleigh one and can essentially limit the working range from the short wavelength side. Another important issue is to check the quality of the holographic layer, in particular, its homogeneity. To this purpose, we developed a colorimetric method of determination of the wavelength with the digital camera [34-36]. On the other hand, one can check the emulsion homogeneity by the distribution of the light scattering parameters.

The computer model of propagation in a layered medium for one-dimensional case was developed. The case of bleached holograms, where absorption is neglected and the refractive index is not depending from wavelength is included. At the same time is neglected and light scattering. Generalization to the dispersion of the refractive index is not an issue. The model allows determining the amplitude of modulation of the refractive index and effective thickness of the holographic layer by fitting the spectrum of the transmission hologram in the presence of the dip near the resonant frequency.

To measure the homogeneity of response of sensor properties over its surface have been applied the colorimetric method with the help of common camera [34-36]. Spatial inhomogeneity can emerge due either to inhomogeneities of the object under consideration, or to those of the sensor properties. The sensor is a thick layer hologram with width of few tens of micrometers. Its reflection spectrum has the spectral width 5-20 nm. Because of it, one suffices to use response from two color channels.

Hence, the problem is reduced to the following. Assume there is a set of emitters on a plane. We are interested in obtaining the spectra of each emitter preferably simultaneously. It is not easy especially if the sources are closely packed and produce almost continuous radiating surface. The situation is simpler if radiation from each point is spectrally narrow. Then, the distribution of the average radiation wavelength over the surface can be found by the colorimetric method. At each surface point one should determine with the required resolution the magnitudes of three components of a colour vector, i.e., obtain a colour image of the surface under study. Presently, the solution of this problem by using digital devices has no principal difficulties. The aim of our work is to solve the problem by means of conventional digital cameras. Each pixel of the colour image presents a particular colour vector in the RGB system. In order to find the distribution of the average wavelength from the image it is necessary to know how the particular digital camera represents radiation of different wavelengths.

The colorimetric method [34, 35] suggested for finding this distribution is as follows. Radiation passes to at least two detecting channels differing in spectral sensitivity. If in a certain spectral range (call it the working range) the ratio of spectral sensitivities of at least two channels is monotonous then one can determine the average wavelength of narrowband radiation from the signal ratio in the channels (see Fig. 12). At the selective sensitivity of the i-th channel $S_i(\lambda)$ its signal is $J_i=\int d\lambda\ S_i(\lambda)\Phi(\lambda)$, where $\Phi(\lambda)$ is the source brightness. For the δ-shape spectral source with brightness Φ_0, which emits at the wavelength λ_x, the signal in this channel is $J_i=I_0S_i(\lambda_x)$. If the ratio of the spectral sensitivities for two chosen channels is $a(l)$, then the sought-for wavelength is the solution of the equation $\alpha(\lambda)=S_1(\lambda)/\ S_2(\lambda)$:

http://dx.doi.org/10.5772/53564

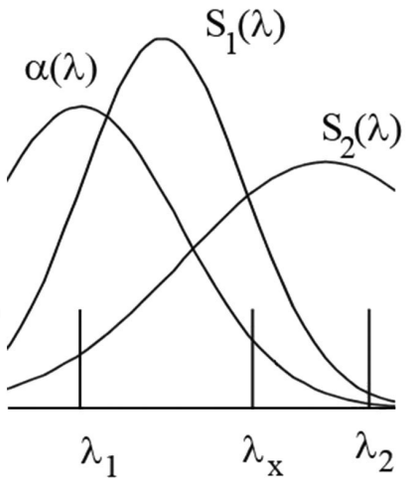

Figure 12. Qualitative view of the spectral sensitivities $S_1(\lambda)$ and $S_2(\lambda)$ of working channels and their ratio $\alpha(\lambda)$: λ_1 and λ_2 are the limits of working range, λ_x is the wavelength of a monochromatic radiation source.

$$\lambda_x = \alpha^{-1}(J_1 / J_2).$$

where α^{-1} is the function inverse to $\alpha(\lambda)$. If the sought-for wavelength is outside the working range, i.e., outside the range of monotonous ratio of sensitivities in two channels, then the unique wavelength determination necessitates an additional (third) channel.

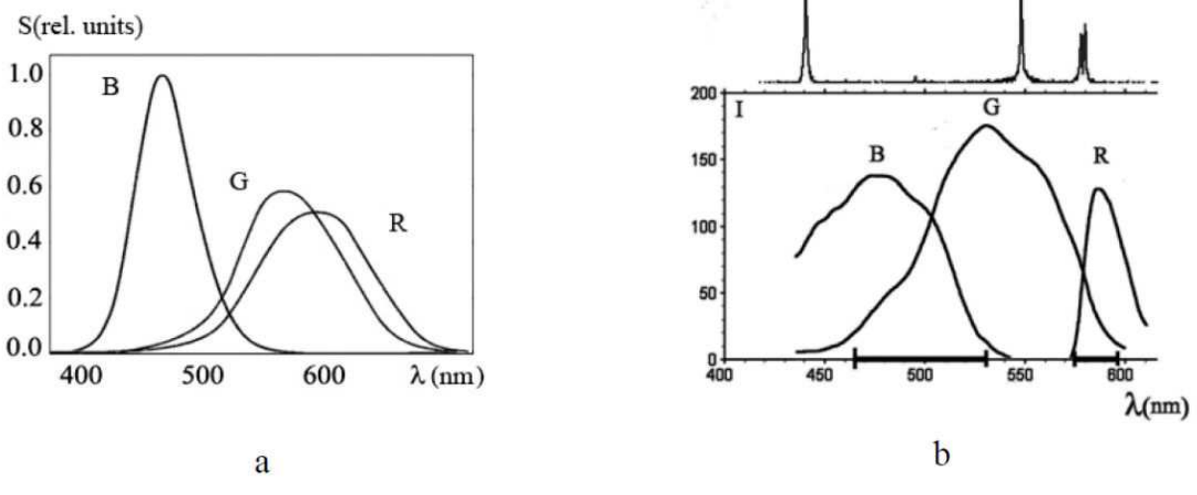

Figure 13. a). The spectral sensitivity of the human eye: signals of red (R) green (G), and blue (B) receptors [37].b). The spectrum of the mercury lamp (top) and signals of red (R), green (G), and blue (B) sensors of Sony F717 digital camera obtained from the photograph of the incandescent lamp spectrum taken by a colour digital camera (bottom).

The case of a finite spectral width is not as simple as that of a δ-like source. In our case the spectrum of reflection from a holographic layer may widen due to several reasons. First, due to a small number of efficiently reflecting layers, which can be related either to a small thickness of the holographic layer or to a short depth of radiation penetration into the layer because of the high reflection caused by high amplitude of the variable part of refractive index or by strong scattering of light. Second, the spectrum may widen due to the non uniform periodicity of layers in depth. We are interested in layer swelling, which is a reason for period variations and is related to the position of reflection maximum. In the latter case it is important to find the average period of layers, which is related to some average wavelength. Obviously, at moderate broadening this parameter can also be determined by means of the procedure described above using the signal relation in different spectral channels. However, in the general case the period obtained in this way from the position of maximum in the measured reflection spectrum differs from the average period. The difference depends both on a particular shape of reflection spectrum and on spectral sensitivities of the channels. The criterion for acceptable line broadening should be the permissible distinction of determined average period from its actual average value. If the sensitivity of sensors is almost constant within the line width of radiation illuminating a single pixel of the array, then radiation actually behaves as monochromatic one. If the spectral sensitivities of the sensor linearly vary within the width of the line that is symmetrical in shape, then the average period determined is the same as that in the case of a monochromatic source. If this condition is ruled out, then in the general case the determined wavelength is distinct from average one.

In the general case, the colorimetric measurements imply a projection of the surface under study to the detecting array through two (or, for expanding the range, a greater number) types of light filters, i.e., it is necessary to create a colorimetric device with a sufficient spatial resolution. A digital camera is just such a device.

In Fig.13a, the spectral sensitivities are shown for three types of human eye cones responsible for colour recognition [37]. A digital camera also distinguishes colours but the spectral sensitivity of its sensors is distinct. For example, we will show below that in the spectral range 540 – 575 nm a digital camera does not discriminate different colour hues at all. In Fig. 13b, the signals of red (R), green (G), and blue (B) sensors of Sony F717 digital camera are shown that were obtained from a digital photograph of the incandescent lamp spectrum. The spectrum was detected from a spectrograph with a diffraction grating (~ 800 lines mm^{-1}). This and all the following results were obtained at the sensitivity ISO 100 and switched-off automatic white balance. If the emission spectrum under study fits one of the two marked working ranges then the digital camera is appropriate for measurements. Note that we studied about ten various cameras and have found that their sensor characteristics are qualitatively similar. Figure 14 shows how a continuous spectrum (colour hue) is represented by digital cameras of various brands. Nevertheless, we did not study the characteristics of particular cameras as we wanted to understand the situation as a whole. Only the basic working Sony F717 digital camera was thoroughly studied. The spectrum of the incandescent lamp with an added calibrating spectrum of the mercury lamp was photographed. The shots used for the comparison were not overexposed, i.e., the maximal signal amplitude in

http://dx.doi.org/10.5772/53564

channels was not above 150 – 200 digital units (the maximal admissible signal is 255 digital units). The colour hue H was determined in a standard way as the polar angle in the cylindrical coordinate system of a three-dimensional colour space. Its value was from 0 to 360. For convenient work in red, green, and blue colour ranges we chose the reference point for the colour hue in the blue range (H = 0 at R = 0, G = 0, B = 255). In this case, the break of the colour hue (0 – 360) fits the blue range and introduces no additional difficulties in data processing. The purely red colour (R = 255, G = 0, B = 0) corresponds to H = 120 and purely green colour (R = 0, G = 255, B = 0) corresponds to H = 240. A more thorough analysis of various digital cameras is interesting but is beyond the framework of the present paper. Anyway, some general information may be obtained from Fig. 13. The principal conclusion important for our work is that all the digital cameras used have a defect of colour sensitivity in the green range.

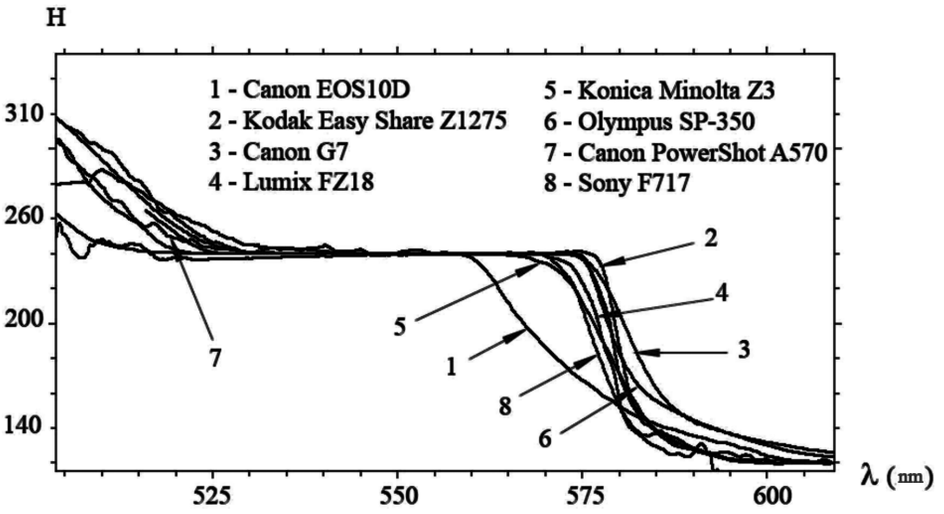

Figure 14. The colour hue (H) versus wavelength for some digital camera types.

Some modern cameras provide the possibility for extracting unprocessed data in the RAW format. Preliminary experiments show that the situation with the colour sensitivity in this case is better. The processor of the digital camera does not distort data but further investigations are necessary for using the RAW format. At the first stage, we limited our study to simplest (mass) formats (JPEG, BMP) by the following reasons. Creation of holographic sensors was assumed for mass consumer and our aim was to develop not only a simple method for checking the quality of sensors but for reading data from them also. The method should be available for mass users, i.e., should rely on simplest digital cameras, in which the RAW format is not presented now. In addition, the processing of the image of the holographic sensor surface should be maximum simple.

A particular procedure for camera spectral calibration was developed because the responses of the three sensor types of the detecting array intricately depend not only on the radiation wavelength but on the exposure as well. The camera to be calibrated takes shots of a continuous spectrum superimposed on the mercury lamp spectrum with various exposures. Then, this spectrum is used for calibrating each image with respect to the wavelength. The images calibrated in this way are then processed together. The result is information on the relationship between the wavelength and sensor responses. The range 570 – 605 nm is considered in which the red and green sensors are sensitive. The signal in the blue channel in this range is not above the noise level. On the basis of all the obtained dependences the characteristic surface is plotted for the camera under study, which gives the sought-for wavelength as a function of the colour hue and the average value of *I*. Once the characteristic surface is plotted the camera can be used as a spectral device in the working range of wavelengths and sensor responses. Applicability of the method was verified on the yellow doublet of the mercury spectrum and on a continuous spectrum of the incandescent lamp (sees Fig. 15). Clearly visible color distortion of the short wavelength doublet line (too green hue, what can assess spectroscopist) in the picture are associated with the mention above defect of JPEG-format of digital camera.

Note that in the case of the mercury spectrum image and continuous spectrum of the incandescent lamp each pixel is illuminated by an almost monochromatic light source, because the fraction of the continuous spectrum per single pixel of the image is less than 1 nm. Having processed the image of spectrum (in Fig. 15a, the domain is shown fitting the working wavelength range) we obtain the map of the wavelength distribution over the image (Fig. 15b); only the image domains from the processing system working ranges are taken into account. Domains with too low values of *I*, in which the signal is close to noise, are neglected. Also neglected are the domains with high *I* in which, probably, noticeable redistribution of signals over different colour channels occurs and domains with almost a zero sensitivity of one of the two sensors. This explains the complicated contour of the wavelength distribution map over the image in the continuous spectrum range. It is interesting that due to different intensities of sources one can see in Fig. 15a the domain with superimposed continuous spectrum and mercury lines. On the wavelength distribution map there is no such superimposed domain, which proves that the recovered wavelengths are equal despite the different intensities. In Figs 15c and d the distributions of various characteristics are shown for horizontal cross sections of the image. It is known that a spectral device with a diffraction grating has a linear dispersion, i.e., the wavelength should linearly vary with the coordinate (Fig. 15d), whereas the colour hue changes obviously nonlinearly (Fig. 15c). The distribution columns (Figs 15e, f, g, and h, i, j) correspond to vertical cross sections of the image along the yellow doublet lines. In Figs 15e and h, the responses of red and green sensors are presented varying along the coordinate in a vertical cross section according to changing *I*. The colour hue H also varies despite the constant wavelength (Figs 15f, i). Nevertheless, in vertical cross sections of the wavelength distribution map coinciding with the mercury spectrum lines (579 nm and 577 nm) the recovered wavelength is constant to a high accuracy both in the domain of mercury lines and in continuous spectrum (Figs 15g and j).

http://dx.doi.org/10.5772/53564

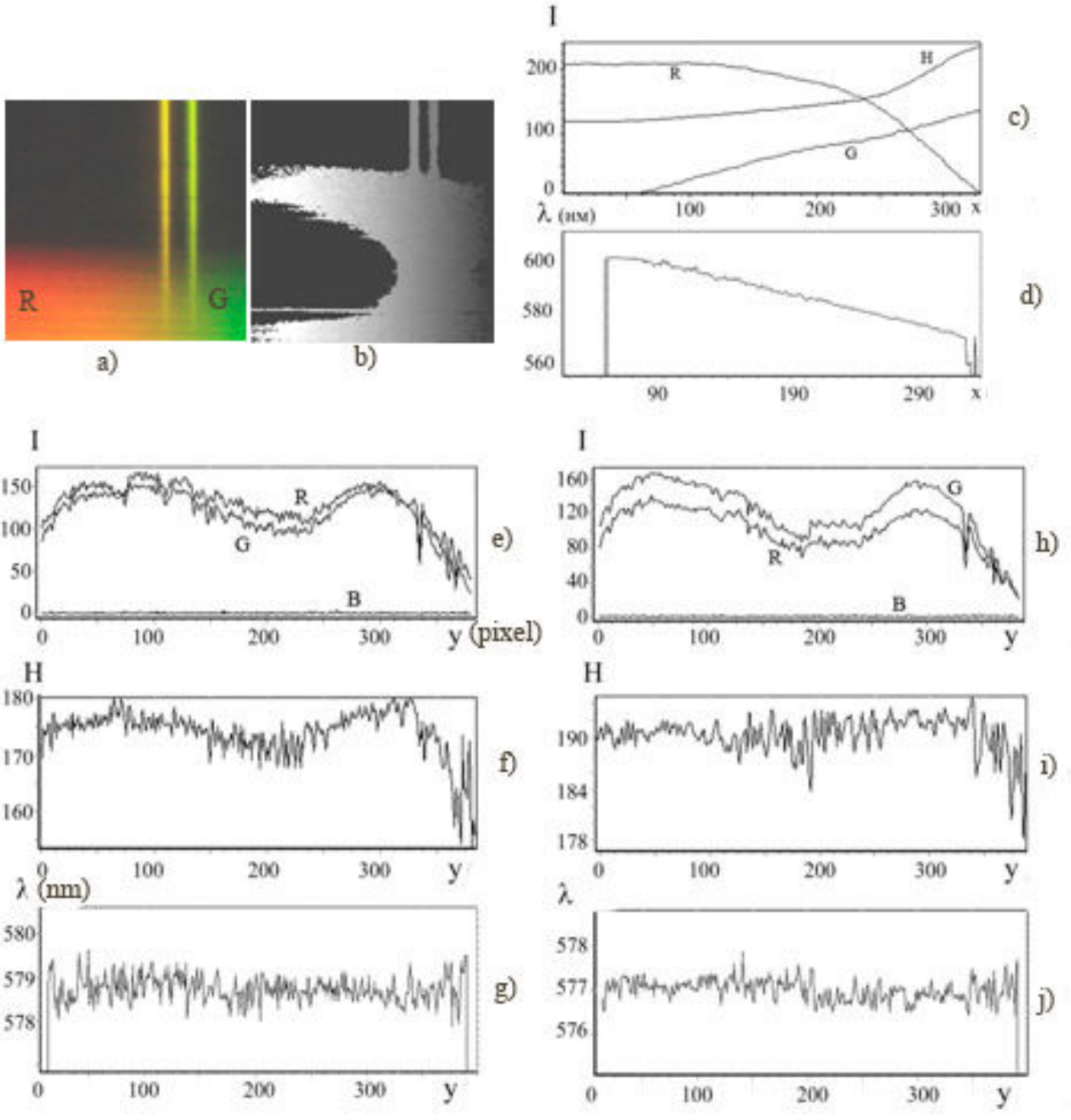

Figure 15. Illustration for an operating test of the method. Shot of spectrum fragment (a); the map of wavelength distribution over the image (b); the distribution of signals in red (R) and green (G) channels and colour hue (H) in a horizontal cross section of the shot (c); the horizontal cross section of the wavelength map (d); the distribution of signal in colour channels (e, h), colour hue (f, i), and calculated wavelengths (g, j) in a vertical cross section of the shot along the mercury doublet lines 579 nm (e, f, g) and 577 nm (h, i, j). The black color on the wavelength map marks the domains in which the signals are beyond the working range and, hence, are excluded from calculation.

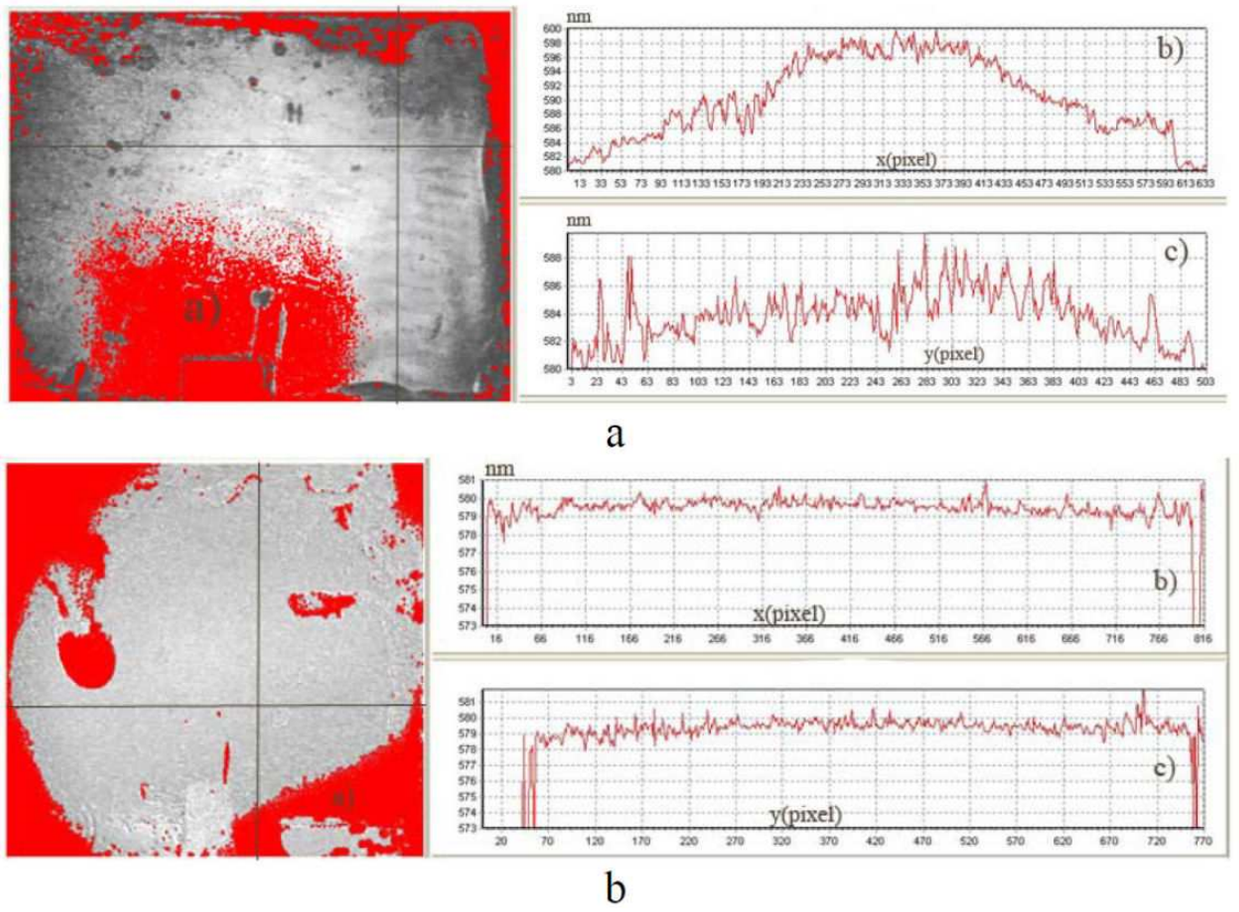

Figure 16. a)The map of wavelength distribution over image (a) and its horizontal (b) and vertical (c) cross sections for a transient process of holographic layer shrinking and b) for a stationary state of sensor AA-AMPh-bis – 87-12-1 mol. %.(JPEG-format) The lines on the maps show the cross-section directions.

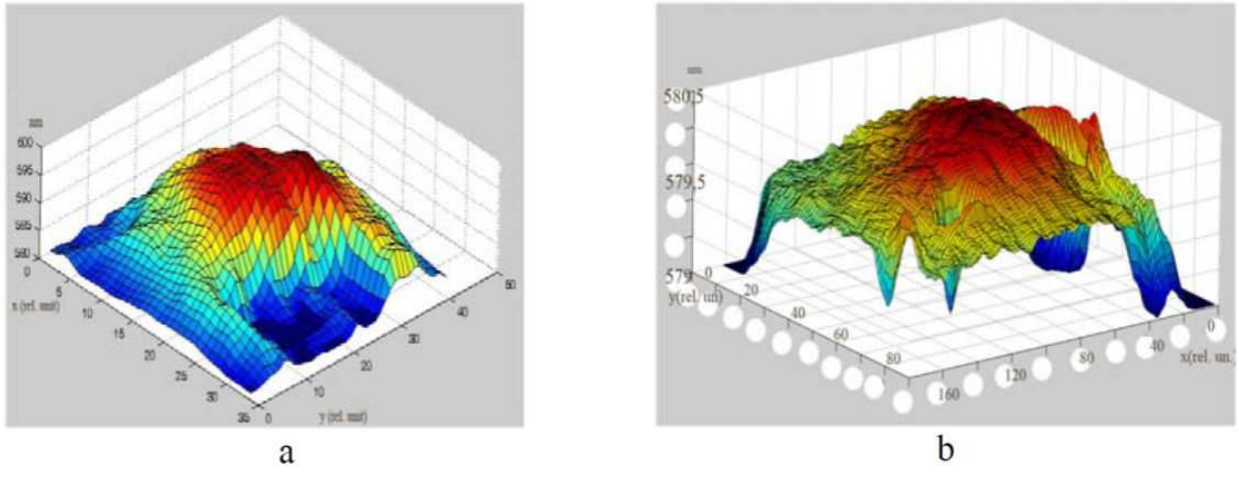

Figure 17. Isometric presentation of the wavelength distribution map (a) in the case of transient shrinkage of the holographic layer of sensor AA-AMPh-bis – 87-12-1 mol.% and for the hologram in a stationary state (b).

http://dx.doi.org/10.5772/53564

By the digital image of the mercury spectrum for the yellow doublet lines and for underlying continuous spectrum we determined the standard deviation of the recovered wavelength in the limits of a narrow window oriented along the central (with respect to the spectrum) part of the mercury line. The window width was 4 pixels, which was less than the line width. The window height was 350 pixels and covered almost all the image of the mercury line and the whole corresponding part of the continuous spectrum. For the mercury doublet lines the wavelengths of 577 nm (the standard deviation is 0.16) and 579 nm (the standard deviation is 0.19) were obtained.

The developed method was employed for studying holographic sensors. The results are shown in Figs 16, 17. The spectrum of radiation reflected from a holographic sensor is wider and the problem of possible inaccuracy in determining the wavelength requires particular investigations. One should keep in mind that in using holographic sensors it is important to know the shift of the wavelength under the action of solution surrounding the sensor rather than the absolute value of the wavelength itself. Data presented in Figs 16a and 17a refer to a transient process to the hologram initially reflecting in the red range. Data for this hologram in ending stationary state is presented in Figs.16b. and 17b. One can see that the spread of wavelengths is noticeably reduced as compared to the transient process, and is less than 2 nm over the whole sensor surface. The local spread also strongly reduced and was less than 1 nm. The map comprises approximately 500 000 points.

The hologram quality and uniformity of the processes occurring during swelling can be estimated from their noise characteristics. In Fig. 18, the standard deviation of the calculated wavelengths is shown versus the width of the averaging window. The standard deviation of wavelength from mean $\bar{\lambda}$ is:

$$A_k = \sqrt{\frac{\sum_i^m (\lambda_i - \bar{\lambda})^2}{m}}$$

where λ_i is the calculated wavelength in the i-th pixel of the image and m is the number of points fitting the window, was averaged over N image points covering the whole studied domain of the sensor. The parameter $S = \frac{1}{N}\sum_k^N A_k$ we will term the noise value. Data presented in Fig. 18 correspond to variation of m from 4 to 2500 pixels. The standard deviation was averaged over the image domain of 500x500 points. With increasing m in the transient process the standard deviation varied from 0.5 to 1.8 nm. A steady increase in noise with the increasing window is related to a large-scale hologram inhomogeneity. In the steady state it was 0.16 – 0.32 nm at the same values of m. An increase in noise at the initial part of the dependence is explained by small-scale inhomogeneity, and the saturation at large m is related to the absence of large-scale inhomogeneity. The ratio of nonstationary noise to stationary level in this range of m increases from 3.4 to 5.6. These facts bear witness that, first, the hologram in the steady state is highly uniform and, second, variations of its swelling over the surface in the nonstationary state are noticeably inhomogeneous.

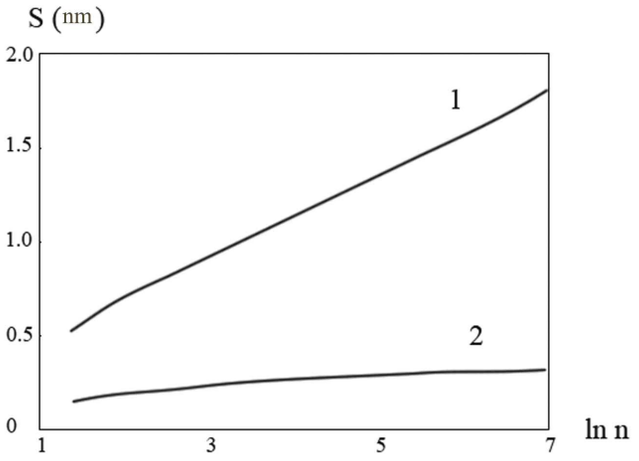

Figure 18. The standard deviation of the calculated wavelength versus the number of points in the averaging window for the transient process (1) and stationary sensor state (2).

Further development of the colorimetric method with the use of RAW-format can significantly increase the working range of wavelengths (440-620 nm), which can be seen from Fig. 19.

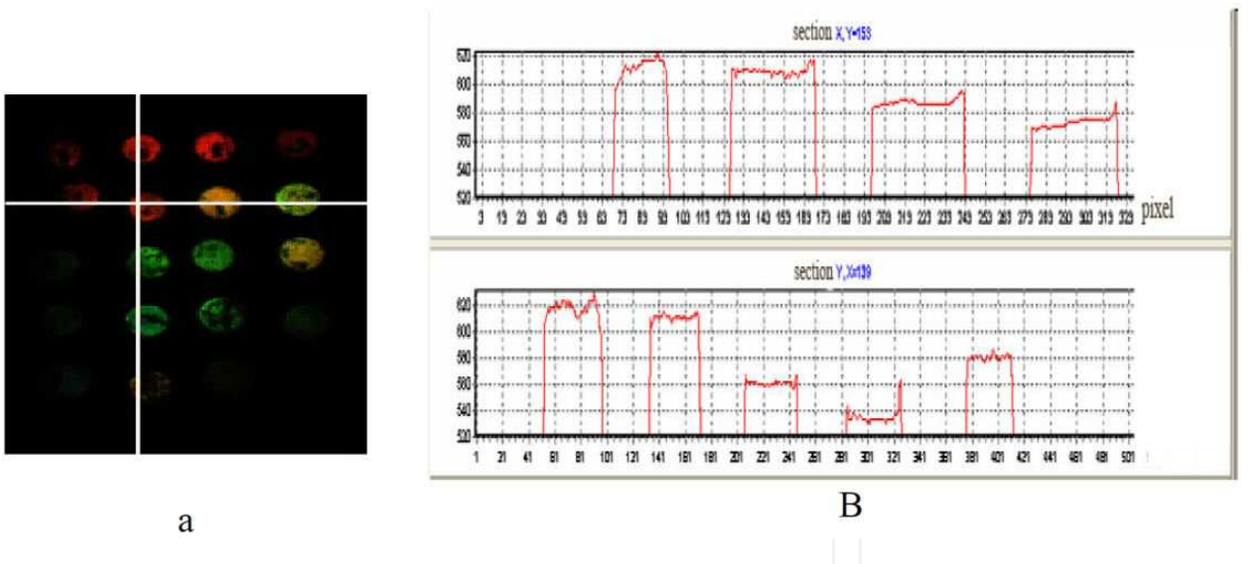

Figure 19. a) The photograph of the hologram in the steady state. b) In the upper right-hand column shows the horizontal and vertical cross-section of the distribution of responses. (RAW-format)

Thus, here is described the method for measuring the distribution of the average wavelength for narrow-band radiation over the source surface by means of a commercial digital camera. There are the following limitations in using the method (without RAW-format): the radiation spectrum should be narrow (the average wavelength is determined); measurements are performed in the spectral range in which at least two sensor types of detecting array are simultaneously sensitive (for the most of cameras

http://dx.doi.org/10.5772/53564

studied these ranges are 470 – 540 nm and 570 – 600 nm). The accuracy of the determined wavelength is not worse than 1 nm. The method was tested on the yellow doublet of the mercury spectrum and on a continuous spectrum of the incandescent lamp covering the working interval 570 – 600 nm. By using this method the uniformity of holographic sensor swelling was studied both in a stationary state and in dynamics.

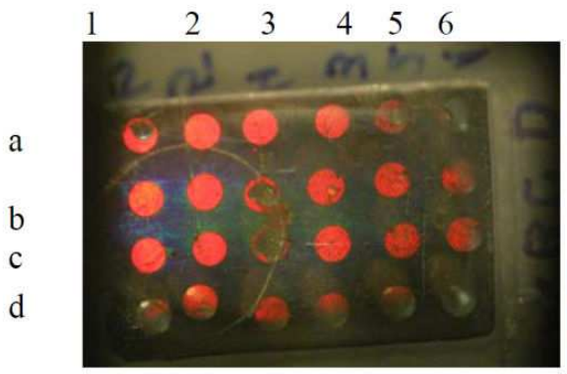

a

	AcOH					
	1	2	3	4	5	6
a	645,6	642,4	643,1	641,0	640,6	643,4
b	645,4	640,6	641,7	640,9	640,6	641,4
c	645,4	644,0	641,1	640,4	640,6	642,2
d	644,5	642,6	641,2	642,6	640,1	641,9
Mean, nm						
642,2	645,2	642,4	641,8	641,2	640,5	642,2
±1,7	0,5	1,7	0,9	1,0	0,3	0,8

b

Figure 20. a) The photograph of the hologram. b) The distribution of samples of 0.5% acetic acid on the sensors surface and wavelength of reflected light in cells (fiber-optic spectrometer).

The design of holographic sensors allows their use in multi-channel mode, when one sensor can simultaneously analyze multiple samples of the same type or define a few parameters of a sample. The holographic sensor is actually a thick hologram plane mirror about the size of a square centimeter. By placing such plate in a special cuvette, containing 24 cells of 2 mm diameter, each contains 50 μL of fluid to be analyzed; it can be used in a multi-channel mode for the simultaneous determination of all samples. The response of the sensor - the wavelength of reflected light - from the cell is easily determined by means of small-sized fiber-optic spectrometer (Fig. 20, 21) or in combination with the developed colorimetric method; it can greatly simplify and speed up the analysis (Fig. 19). As can be seen from Fig. 20, the wavelength of the reflected light at different points on the surface is almost the same (the standard deviation is 1.7 nm). This way you can see the spatial pattern of

kinetics of the holographic sensor, to conduct research of the spatial distribution of processes, with the help of special devices to conduct simultaneous analysis of different components or different samples. Fig. 21 presents the results of the determination of glucose in the blood serum of diabetic patients with glucose sensor (see Fig.) based on aminophenylboronic acid. Despite a significant decrease in the sensitivity of the sensor to the glucose concentration in blood plasma, determined by glucose clearly distinguished spectrometrically.

	1	2	3	4	5	6
a	AcOH	3,32	4,86	9,90	-	AcOH
b	AcOH	3,32	4,86	9,90	-	AcOH
c	AcOH	AcOH	AcOH	9,90	-	AcOH
d	AcOH	3,32	4,86	9,90	-	AcOH

a

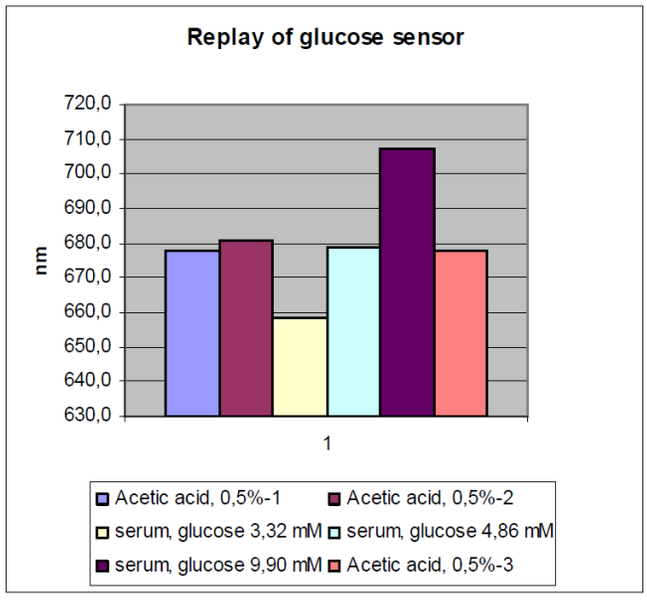

b

Figure 21. a). The distribution of blood serum (*) [glucose], mM) samples with different glucose concentrations and 0.5% acetic acid on the sensors surface. b). Response (λ_{nm}) of glucose sensor (AA-GA- AMPh - bis: 87,5 - 6 – 6 - 0.5 mol. %) (fiber-optic spectrometer).

3. Conclusion

Thus, we have developed a colorimetric method of determination of the wavelength with the digital camera to study processes in inhomogeneous systems and to check the quality of the holographic layer. On this basis we revealed the multichannel simultaneous methods of analysis of spatially inhomogeneous objects and processes. We have found that the change in the ionic composition of solution is accompanied by the change in the distance between silver nanograin layers and in the diffraction efficiency of holograms. Based on this, we are formulated conditions for optimization of the operating mode of the holographic layer. Transition processes revealed variations in the reflection line shape, caused by the inhomogeneity of the sensitive layer, and non-monotonic changes in the emulsion thickness and diffraction efficiency. In this relation it was developed the computer model of propagation in a layered medium for one-dimensional case 33.

We have developed the method for manufacturing holographic sensors of different types and selected the composition of components of the hydrogel medium for the systems that can be used as bases for glucose sensors. The maximum mean holographic response in the mmol·L^{-1} region concentrations of glucose (1-20 mmol·L^{-1}) per 1 mmol·L^{-1} of glucose in model solutions achieves ~40 nm/(mmol·L^{-1}). It has been shown that holographic sensors can be used to determine the quality of water, in particular, for drinking, the acidity of media, ethanol concentration, ionic strength, metal ions and glucose in blood serum.

http://dx.doi.org/10.5772/53564

Acknowledgements

This work was supported by grant of the Program of Fundamental Studies "Fundamental Sciences for Medicine" of the Presidium of RAS.

Author details

Vladimir A. Postnikov[1*], Aleksandr V. Kraiskii[2] and Valerii I. Sergienko[3]

*Address all correspondence to: vladpostnikov@mail.ru

1 Laboratory of Medical Nanotechnology, Scientific Research Institute of Physical-Chemical Medicine, Moscow, Russia

2 G.S. Landsberg Optical Department, P.N.Lebedev Physical Institute of the Russian Academy of Sciences, Moscow, Russia

3 Department of Biophysics, Scientific Research Institute of Physical-Chemical Medicine, Moscow, Russia

References

[1] Millington R, Mayes A, Blyth J, and Lowe C. A Holographic sensor for Proteases. Anal. Chem. 1995; 67,4229-4233

[2] Mayes A, Blyth J, Kyrollo1inen-Reay M, Millington R. and Lowe C. A holographic alcohol sensor. Anal. Chem. 1999; 71, 3390-3396

[3] Holtz J, Asher S. Polymerized colloidal crystal hydrogel films as intelligent chemical sensing materials. Nature. 1997; 389, 829–32.

[4] Reese E, Baltusavich M, Keim J, Asher S. Development of an intelligent polymerized crystalline colloidal array colorimetric reagent. Anal Chem. 2001; 73, 5038–42.

[5] Marshall A, Young D, Kabilan S, Hussain A, Blyth J. and Lowe C. Holographic sensors for the determination of ionic strength. Analytica Chimica Acta. 2004; 527(1), 13-20

[6] González B, Christie G, Davidson C, Blyth J. and Lowe C. Divalent metal ion-sensitive holographic sensors. Analytica Chimica Acta. 2005; 528(2), 219-228

[7] Alexeev V, Sharma A, Goponenko A, Das S, Lednev I, Wilcox C, et al. High ionic strength glucose-sensing photonic crystal. Anal Chem 2003; 75, 2316–23.

[8] Asher S, Alexeev V, Goponenko A, Sharma A, Lednev I, Wilcox C, et al. Photonic crystal carbohydrate sensors: low ionic strength sugar sensing. J Am Chem Soc 2003; 125, 3322–9.

[9] Kabilan S, Marshall A, Sartain F, Lee M.-C, Hussain A, Yang X, Blyth J, Karangu N, James K, Zeng J, Smith D, Domschke A. and Lowe C. Holographic glucose sensors. Biosensors and Bioelectronics. 2005; 20(8), 1602-1610

[10] Yang X, Lee M.-C, Sartain F, Pan X, Lowe C.R. Designed Boronate Ligands for Glucose-Selective Holographic sensors. Chem. Eur. J. 2006; 12, 8491-8497

[11] Horgan A, Marshall A, Kew S, Dean K, Creasey C. and Kabilan S. Crosslinking of phenylboronic acid receptors as a means of glucose selective holographic detection. Biosensors and Bioelectronics. 2006; 21(9), 1838-1845

[12] Worsley G, Tourniaire G, Medlock K, Sartain F, Harmer H, Thatcher M, Horgan A, and Pritchard J. Continuous Blood Glucose Monitoring with a Thin-Film Optical Sensor. Clinical Chemistry. 2007; 53(10), 1820-26

[13] Yang X, Pan X, Blyth J, Lowe C.R. Towards the real-time monitoring of glucose in tear fluid: Holographic glucose sensors with reduced interference from lactate and pH. Biosensors and Bioelectronics. 2008, 23, 899–905

[14] Alexeev VL, Das S, Finegold DN, Asher SA. Photonic crystal glucose-sensing material for noninvasive monitoring of glucose in tear fluid. Clin Chem. 2004; 50, 2362–9.

[15] Bhatta D, Christie G, Madrigal-González B, Blyth J. and Lowe C.R. Holographic sensors for the detection of bacterial spores. Biosensors and Bioelectronics. 2007; 23(4), 520-527

[16] Bhatta D, Christie G, Blyth J, Lowe C.R.. Development of a holographic sensor for the detection of calcium dipicolinate-A sensitive biomarker for bacterial spores. Sensors and Actuators. 2008; B 134, 356–359

[17] Marshall AJ, Young DS, Blyth J, Kabilan S, and Lowe CR. Metabolite-Sensitive Holographic Biosensors. Anal. Chem. 2004; 76 (5), 1518-1523

[18] Lee M-C, Kabilan S, Hussain A, Yang X, Blyth J, and Lowe CR. Glucose-Sensitive Holographic sensors for Monitoring Bacterial Growth. Anal. Chem. 2004; 76 (19), 5748-5755

[19] Bell LL, Seshia AA, Davidson CA, Lowe CR. Integration of holographic sensors into microfluidics for the real time pH sensing of L. casei metabolism. Procedia Engineering. 2010; 5, 1352-1355

[20] Naydenova I, Jallapuram R, Toal V, Martin S. Characterisation of the humidity and temperature responses of a reflection hologram recorded in acrylamide-based photopolymer. Sensors and Actuators. 2008; B 139(1) , 35-38

[21] Cody D, Naydenova I, Mihaylova E. New non-toxic holographic photopolymer material. J. Opt. 14 (2012) 015601 (4pp)

[22] Sartain FK, Yang X, Lowe CR. Holographic lactate sensor. Anal Chem. 2006;78(16), 5664-70

[23] Postnikov VA, Kraiskii AV, Sultanov TT, Tikhonov VE. Hydrogel holographic sensors sensitive to an acid media. In Proceedings of XVIII Intenational scool-seminar "Spectroscopy of molecules and crystals" 20.09-28.09.2007, Beregove, Crimea, Ukraine, Abstracts p.261

[24] Postnikov VA, Kraiskii AV, Tikhonov VE, Sultanov TT, Khamidulin AV. Hydrogel holographic sensors for detection of components in biological fluids. In Proceedings of CAOL 2008: 4th International Conference on Advanced Optoelectronics and Lasers ,2008,), Alushta, Crimea South Coast, Ukraine, September 29 – October 4, art. no. 4671956, 369-371

[25] Postnikov VA, Kraiskii AV, Tikhonov VE, Sultanov TT, Khamidulin AV. Hydrogel holographic sensors for detection of components in biological fluids. In Proceedings of CAOL 2008: 4th International Conference on Advanced Optoelectronics and Lasers ,2008,), Alushta, Crimea South Coast, Ukraine, September 29 – October 4, art. no. 4671956, 369-371

[26] Postnikov VA, Kraiskii AV, Sultanov TT, Deniskin VV. Holographic sensors of glucose in model solution and serum. In Conference Proceedings - 5th International Conference on Advanced Optoelectronics and Lasers, CAOL' 2010, September 10 -14, 2010, Sevastopol, Crimea, Ukraine, art. no. 5634191, 257-258

[27] Postnikov VA, Kraiskii AV, Sultanov TT. Holographic sensors. In Conference Proceedings - 11th International Conference on Laser and Fiber-Optical Networks Modeling, LFNM 2011, Kharkov, Ukraine, September 5 – 8, 2011, art. no. 6145033, 369-371

[28] Kraiskii AV, Postnikov VA, Sultanov TT, Khamidulin AV. Holographic sensors diagnostics of solution components. Quantum Electronics. 2010; 40 (2), 178 -182

[29] Hansen J, Christensen J, Petersen J, Hoeg-Jensen T, Norrild J. Arylboronic acids: A diabetic eye on glucose sensing. Sensors and Actuators. 2012; B 161, 45– 79

[30] Steiner M-S, Duerkop A, Wolfbeis O. Optical methods for sensing glucose. Chem. Soc. Rev. 2011; 40, 4805–4839

[31] Christopher R. Cooper and Tony D. James. Synthesis and evaluation of D-glucosamine-selective fluorescent sensors. J. Chem. Soc., Perkin Trans. 2000; 1 ,963–969

[32] Egawa Y, Seki T, Takahashi S, Anzai J-i. Electrochemical and optical sugar sensors based on phenylboronic acid and its derivatives. Materials Science and Engineering 2011; C 31, 1257–1264

[33] Kraiskii AV, Postnikov VA, Sultanov TT, Mironova TV, Kraiskii AA. On optical properties of holographic sensors based on silver emulsions. In Conference Proceedings - 11th International Conference on Laser and Fiber-Optical Networks Modeling, LFNM 2011, Kharkov, Ukraine, September 5 – 8, 2011 , art. no. 5634214, 191-192

[34] Kraiskii AV, Mironova TV, Sultanov TT, Postnikov VA, Sergienko VI, Tikhonov VE. Sposob izmereniya dliny volny…, Pat. RF No. 2390738, prior. 21.05.2008.

[35] Kraiskii AV, Mironova TV, Sultanov TT. Measurement of the surface wavelength distribution of narrow-band radiation by a colorimetric method. Quantum Electronics. 2010; 40 (7), 652 – 658 36.

[36] Kraiskii AV, Mironova TV, Sultanov TT, Postnikov VA. Measuring surface distribution of narrowband radiation wavelength by colorimetric method. In Conference Proceedings - 5th International Conference on Advanced Optoelectronics and Lasers, CAOL' 2010, September 10 -14, 2010, Sevastopol, Crimea, Ukraine, art. no. 5634214, 191-192

[37] Judd D.B., Wyszecki G. Color in Business, Science and Industry (New York: Wiley, 1975; Moscow: Mir, 1978).